Supplementary Information

A Deep Insight to the Exfoliation Properties of MAX to MXenes and Hydrogen Evolution Performances of 2D MXenes

Yuwen Cheng,[1,2] Lijuan Wang,[2] Yan Song,[2, *] Yumin Zhang[1,*]

1 National Key Laboratory of Science and Technology for National Defence on Advanced Composites in Special Environments, Harbin Institute of Technology, Harbin, 150001, PR China

2 School of Materials Science and Engineering, Harbin Institute of Technology at Weihai, 2 West Wenhua Road, Weihai, 264209, PR China
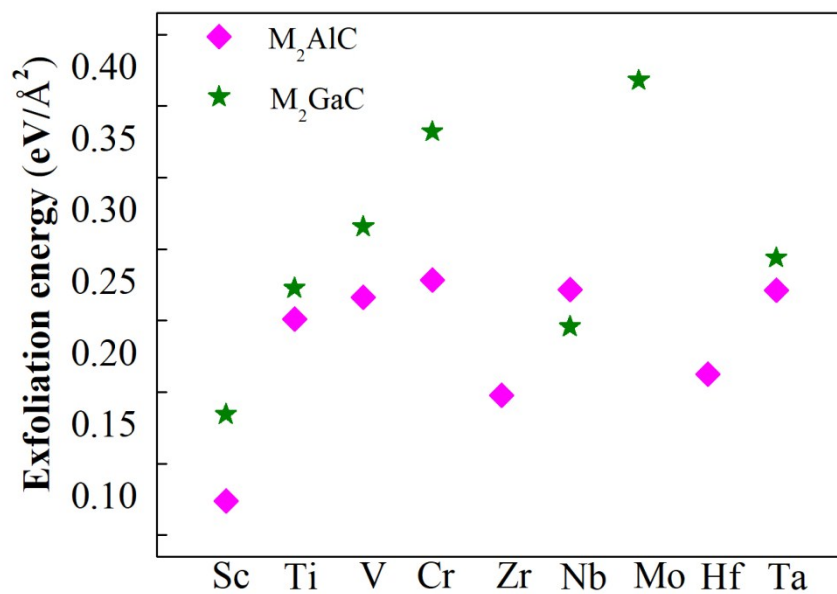
*Corresponding Authors:

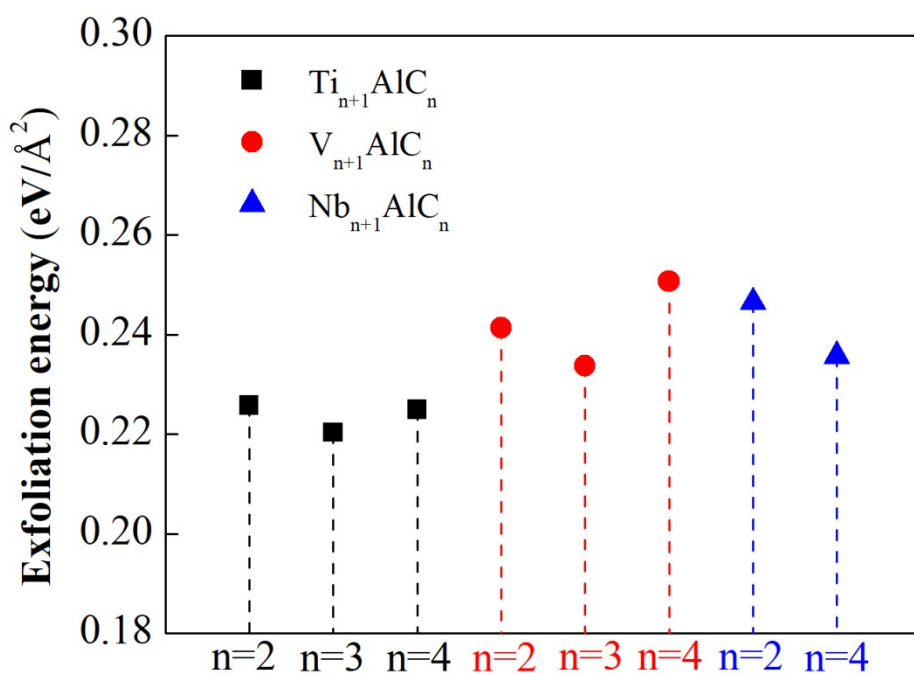E-mail: sy@hitwh.edu.cn (YS); zhym@hit.edu.cn (ZYM)

1. **Figures and Tables**
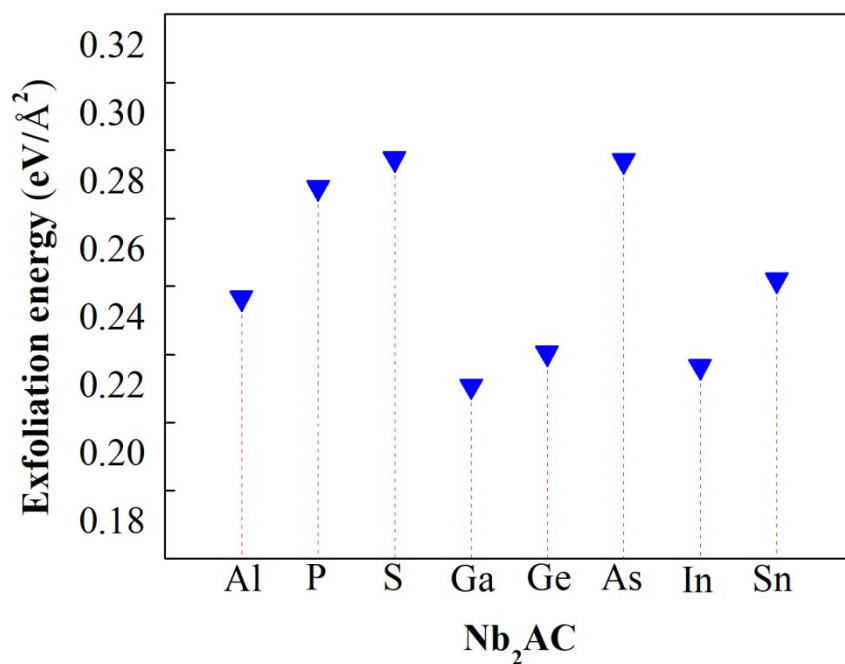
Figure S1. The exfoliation energy of Nb_2AC to Nb_2C (A=Al, P, S, Ga, Ge, As, In, and Sn).

Figure S2. The exfoliation energy of M_2AlC and M_2GaC to M_2C, respectively (M=Sc, Ti, V, Cr, Zr, Nb, Mo, Hf, and Ta).

Figure S3. The exfoliation energy of $Ti_{n+1}AlC_n$, $V_{n+1}AlC_n$ and $Nb_{n+1}AlC_n$ to $Ti_{n+1}C_n$, $V_{n+1}C_n$ and $Nb_{n+1}C_n$, respectively.
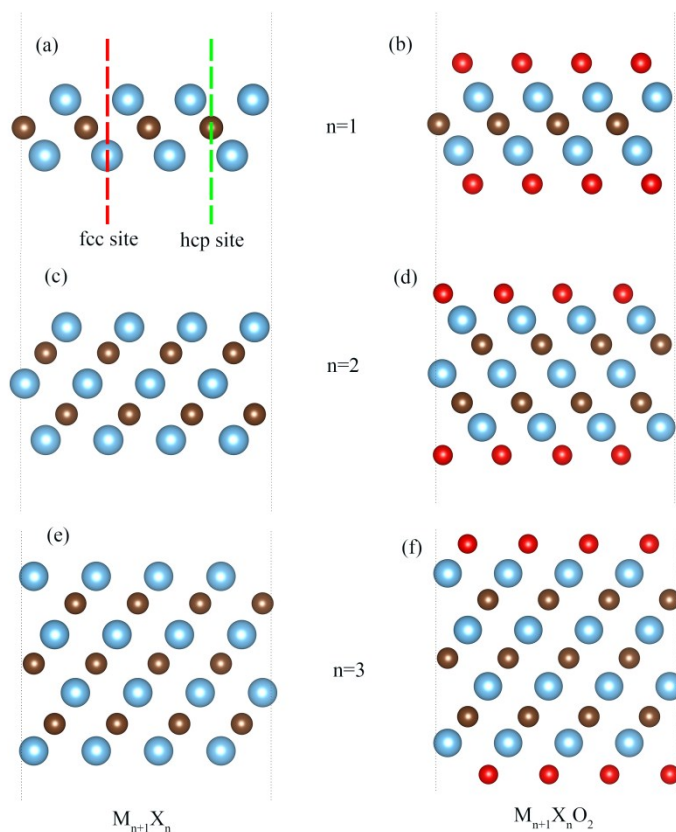
Figure S4. Lattice structures of 2D $M_{n+1}C_n$ (a) M_2C, (c) M_3C_2 and (e) M_4C_3, and of $M_{n+1}C_nO_2$ that

oxygen termination at the fcc site MXenes: (b) M_2CO_2, (d) $M_3C_2O_2$, and (f) $M_4C_3O_2$. Red and green bold dashed lines represent fcc site and hcp site, respectively. Light blue, brown, and red balls represent transition metals, carbon and oxygen atoms, respectively.
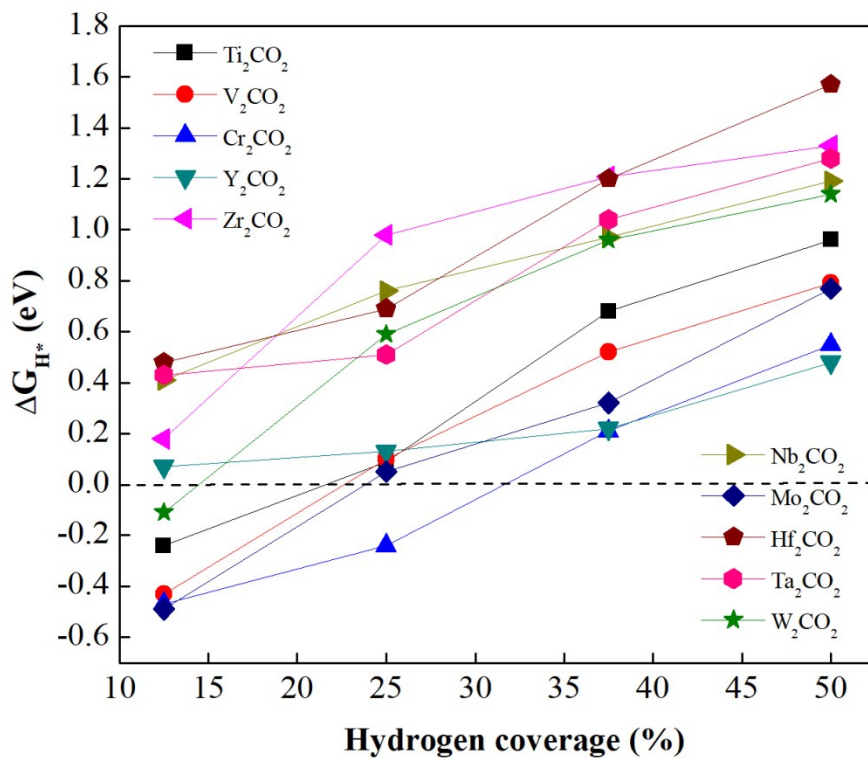
Figure S5. Dependence of hydrogen adsorption free energy (ΔG_{H*}) of studied M_2CO_2 on hydrogen coverages.
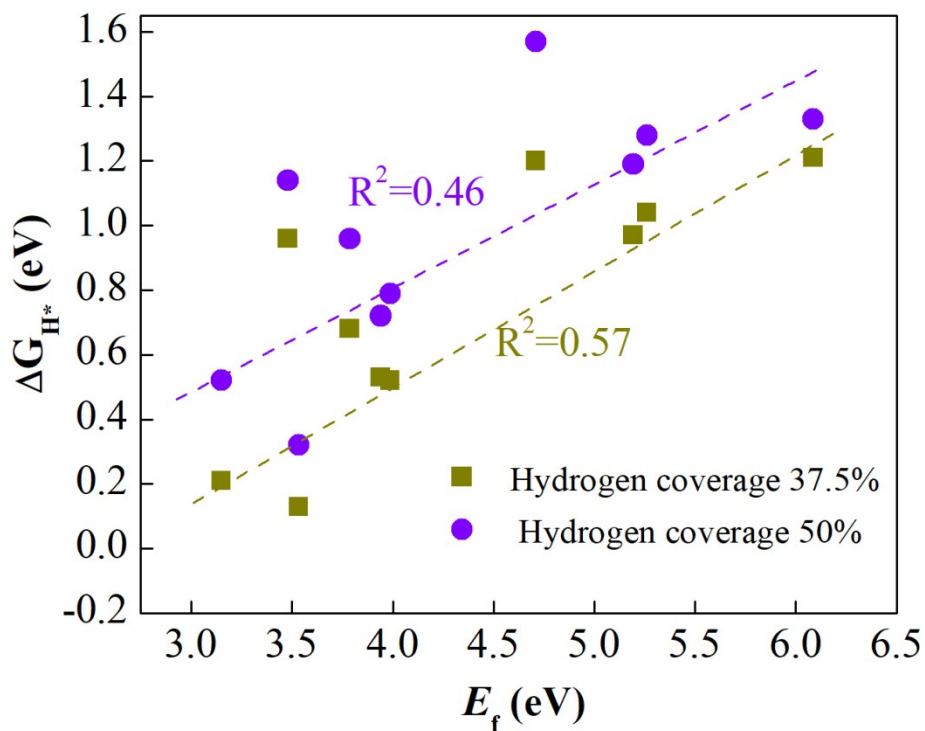
Figure S6. Relationship between ΔG_{H*} and E_f at 37.5 % (dark yellow squares) and 50% (violet balls) hydrogen coverages.
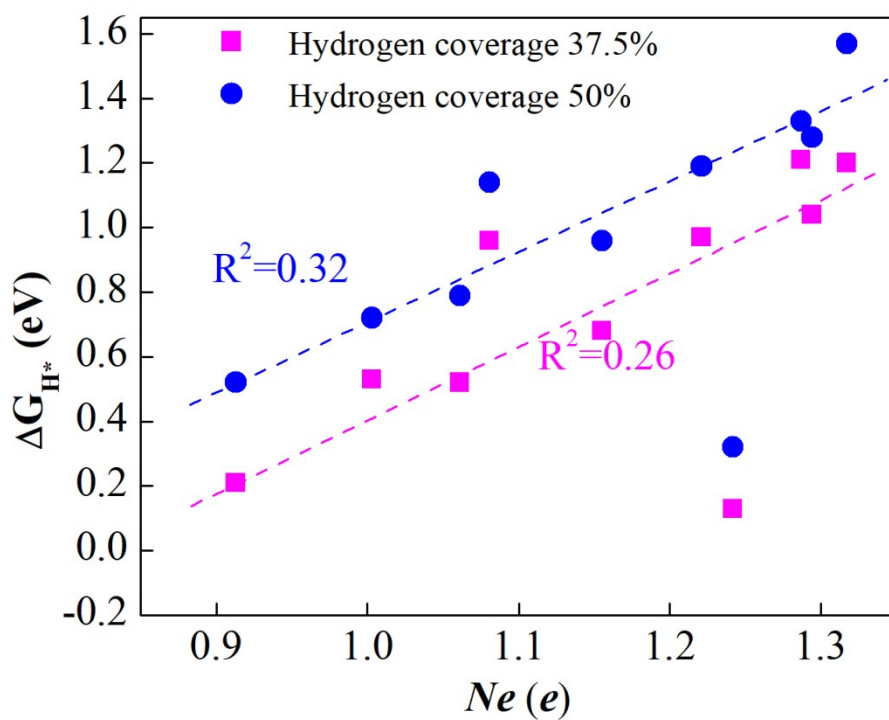
Figure S7. Relationship between ΔG_{H*} and Ne at 37.5 % (magenta squares) and 50% (blue balls) hydrogen coverages.
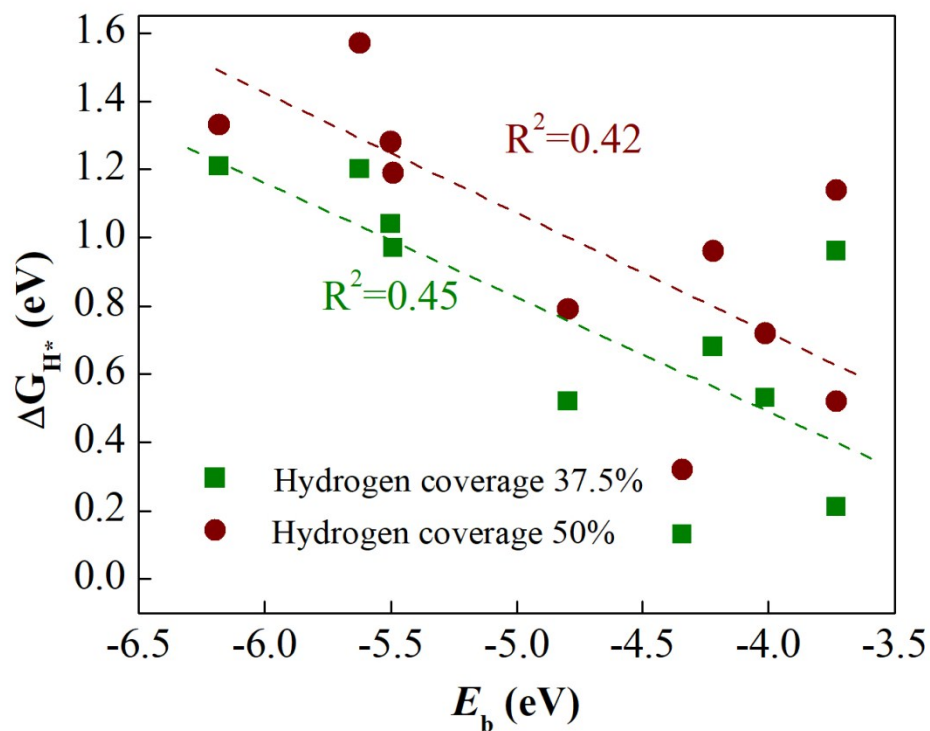
Figure S8. Relationship between ΔG_{H*} and E_b at 37.5 % (cyan green squares) and 50% (wine balls) hydrogen coverage.
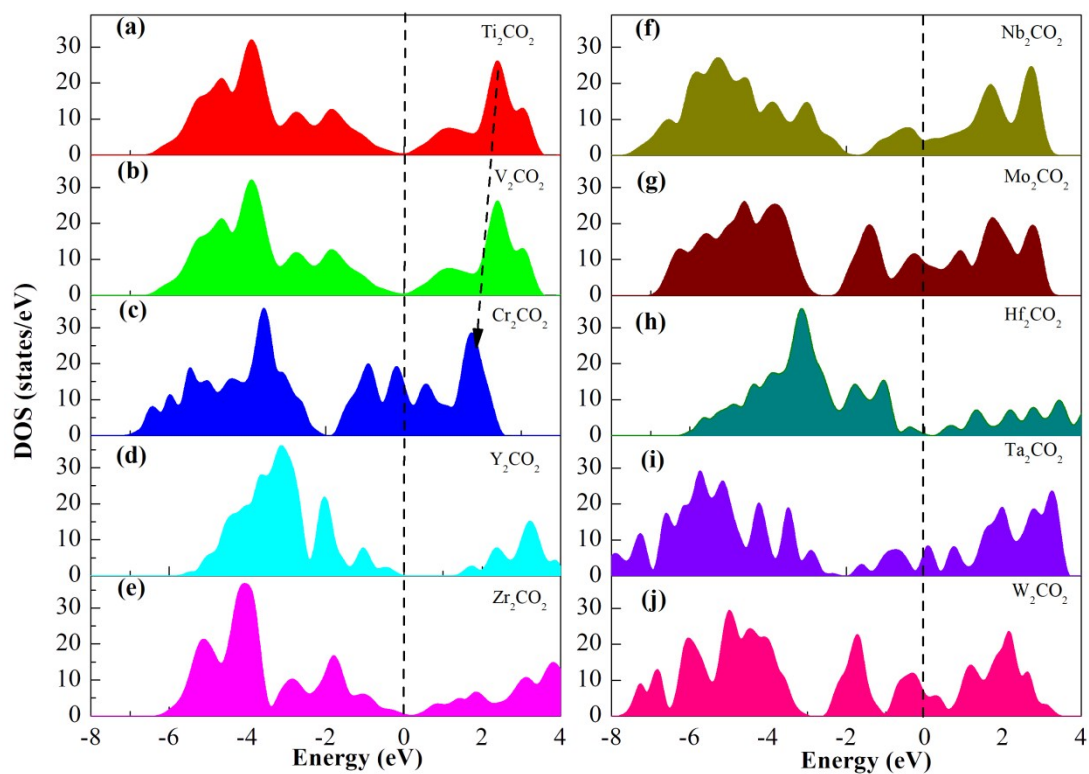
Figure S9. Densities of states of (a) Ti_2CO_2, (b) V_2CO_2, (c) Cr_2CO_2, (d) Y_2CO_2, (e) Zr_2CO_2, (f) Nb_2CO_2,

(g) Mo_2CO_2, (h) Hf_2CO_2, (i) Ta_2CO_2, and (j) W_2CO_2. The dash line represents the Fermi level energy and the dash arrow line indicates that the shifting of DOS to lower energy with the groups increase (such as Ti→Cr).
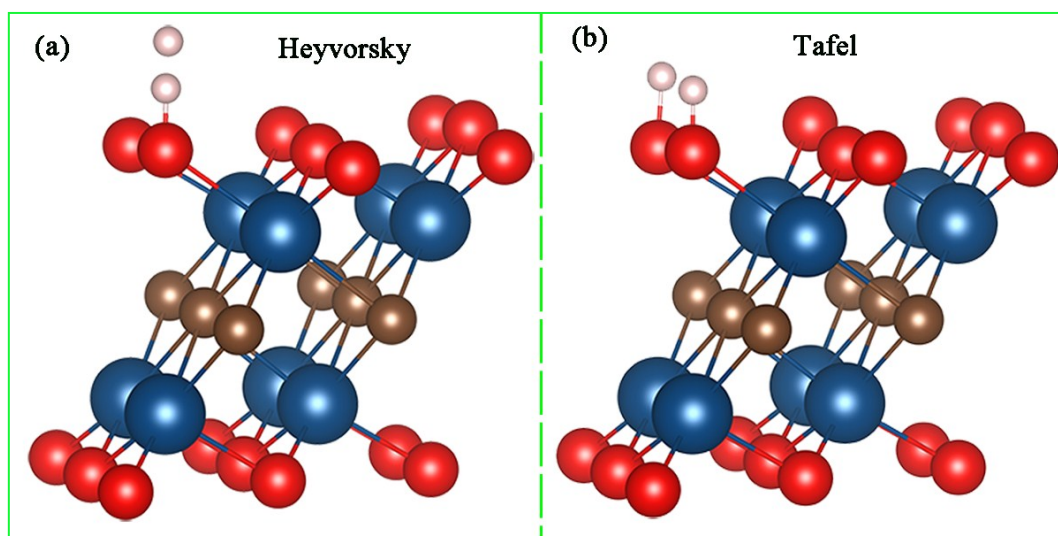
Figure S10. Schematic of Heyrovsky and Tafel adsorptions on M_2CO_2 surface.
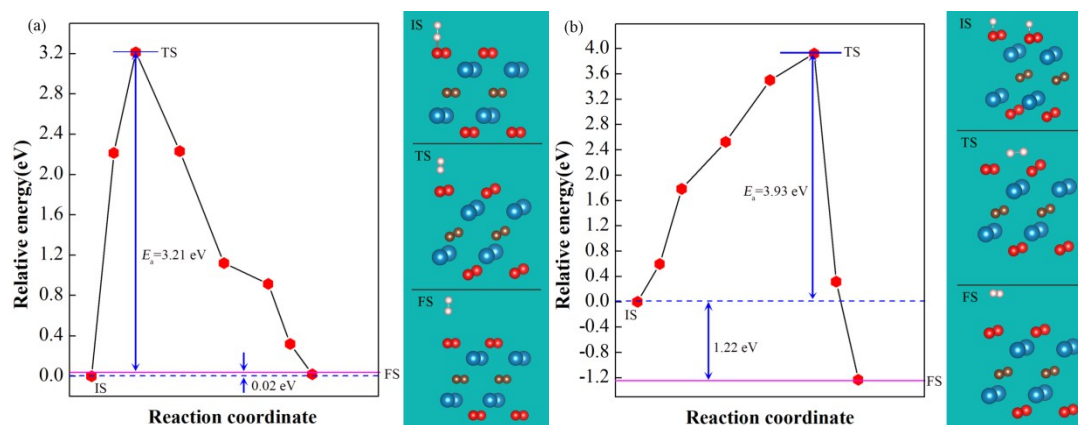
Figure S11. The minimum energy pathway and activation energies of hydrogen desorption from Zr_2CO_2 surface for (a) Heyrovsky reaction and (b) Tafel reaction. The right panels show the initial state (IS), transition state (TS) and final state (FS) of two pathways for reducing protons to hydrogen.
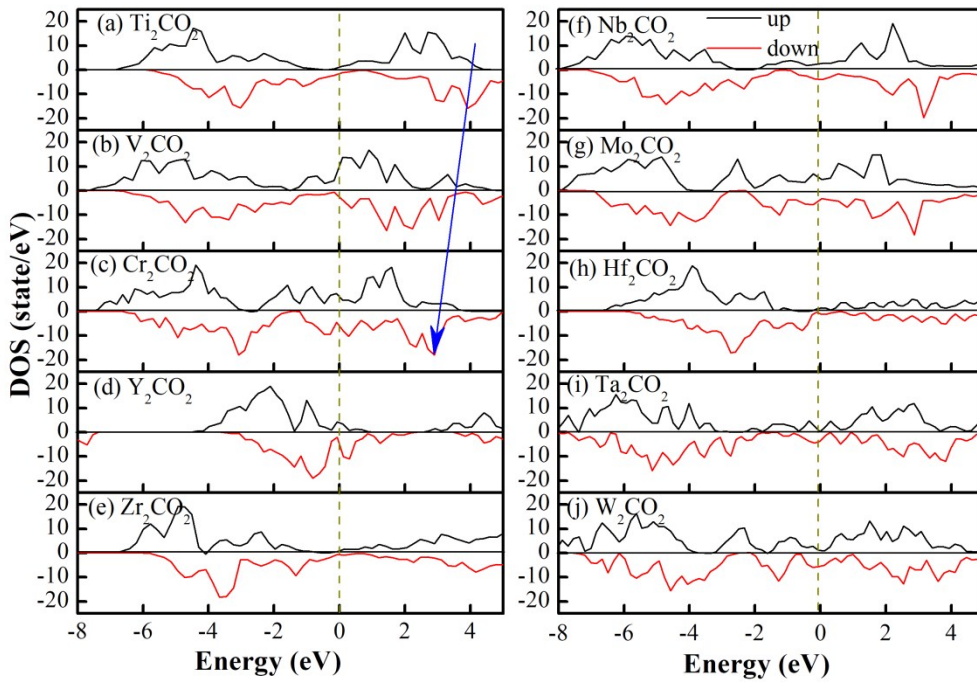
Figure S12. Densities of states (with considering spin-polarization) of (a) Ti_2CO_2, (b) V_2CO_2, (c) Cr_2CO_2, (d) Y_2CO_2, (e) Zr_2CO_2, (f) Nb_2CO_2, (g) Mo_2CO_2, (h) Hf_2CO_2, (i) Ta_2CO_2, and (j) W_2CO_2. The dash line represents the Fermi level energy and the arrow line indicates that the shifting of DOS to lower energy with the increase of groups (such as Ti→Cr).
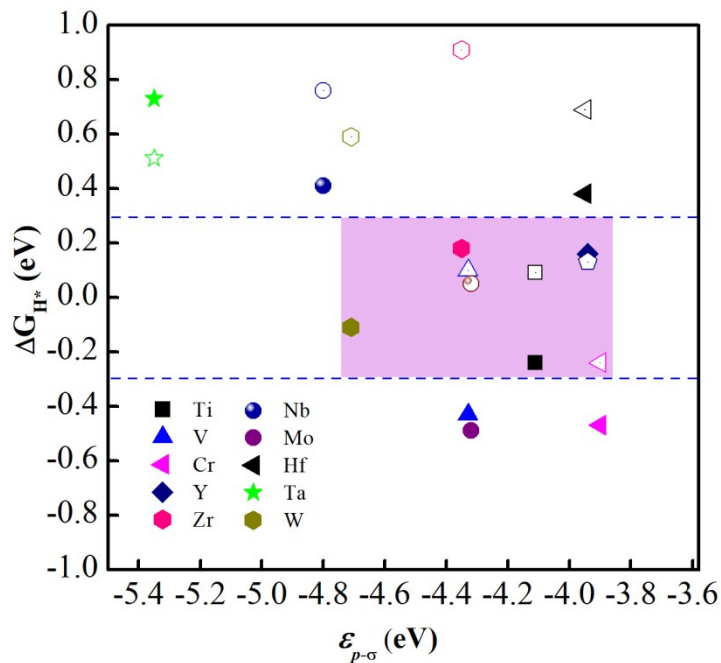
Figure S13. The correlation between adsorption free energy of atomic hydrogen (ΔG_{H*}) and $\varepsilon_{p-\sigma}$, ΔG_{H*} is obtained at hydrogen coverage of 12.5% (solid) and 25% (hollow), respectively.
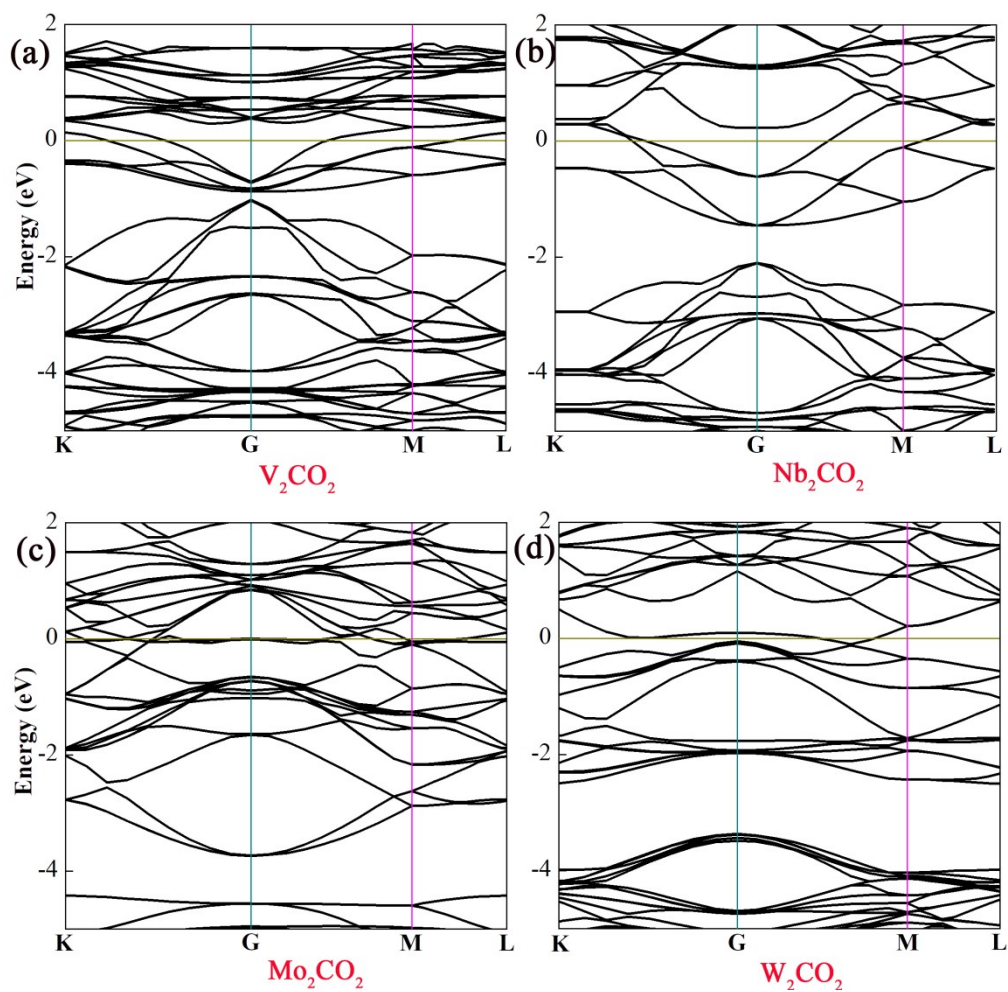
Figure S14. Electronic structures of four kinds of O-terminal MXenes, (a) V_2CO_2, (b) Nb_2CO_2, (c) Mo_2CO_2, (d) W_2CO_2.

Table S1. The lattice parameters of bulk Nb_2AC and bond lengths of Nb-C and Nb-A bonds (A = Al, P, Ga, Ge, or As).

A	a(Å)	c(Å)	c/a	d_{Nb-C}(Å)	d_{Nb-A}(Å)
Al	3.086	13.743	4.453	2.175	2.821
P	3.273	11.537	3.524	2.211	2.565
S	3.282	11.394	3.471	2.195	2.591
Ga	3.278	13.712	4.183	2.252	2.926
Ge	3.377	12.278	3.635	2.289	2.703
As	3.392	11.901	3.508	2.216	2.661
In	3.195	14.539	4.551	2.212	3.042
Sn	3.465	12.820	3.699	2.183	3.124

Table S2. The lattice parameters of bulk V_2AC and bond lengths of V-C and V-A bonds (A = Al, P, Ga, Ge, or As).

A	a(Å)	c(Å)	c/a	d_{V-C}(Å)	d_{V-A}(Å)
Al	2.875	14.578	5.071	1.995	2.536
P	3.044	12.806	4.207	2.055	2.401
Ga	2.884	12.786	4.433	2.009	2.658
Ge	2.994	12.066	4.031	2.014	2.630
As	3.694	13.708	3.711	2.024	2.566

Table S3. The lattice parameters of bulk Hf_2AC and bond lengths of Hf-C and Hf-A bonds (A = Al, In, Sn, Tl, or Pb).

A	a(Å)	c(Å)	c/a	d_{Hf-C}(Å)	d_{Hf-A}(Å)
Al	3.248	14.290	4.399	2.253	2.986
In	3.298	14.843	4.501	2.262	3.126
Sn	3.303	14.482	4.323	2.268	3.059
Tl	3.301	14.838	4.495	2.269	3.129
Pb	3.343	14.877	4.452	2.287	3.147

Table S4. The lattice parameters of bulk Zr_2AC and bond lengths of Zr-C and Zr-A bonds (A = Al, S, In, Sn, Tl, or Pb).

A	a(Å)	c(Å)	c/a	d_{Zr-C}(Å)	d_{Zr-A}(Å)
Al	3.291	14.513	4.409	2.282	3.033
S	3.405	12.898	3.787	2.317	2.664
In	3.233	10.031	3.107	2.149	2.948
Sn	3.341	14.664	4.389	2.299	3.091
Tl	3.760	13.243	3.522	2.335	3.273
Pb	3.383	15.122	4.469	2.324	3.182

Table S5. The lattice parameters of bulk M_2AC and bond lengths of M-C and M-A bonds (M= Cr, Mo, Sc or Ta, A = Al, Ga, Ge, In, or Tl).

M_2AC	a(Å)	c(Å)	c/a	$d_{M\text{-}C}$(Å)	$d_{M\text{-}A}$(Å)
Cr_2AlC	2.829	12.587	4.449	1.923	2.795
Cr_2GaC	2.858	12.397	4.337	1.949	2.641
Cr_2GeC	2.954	12.081	4.089	1.997	2.614
Mo_2GaC	3.059	10.291	3.364	2.134	2.638
Ta_2AlC	3.073	13.802	4.491	2.175	2.801
Ta_2GaC	3.090	13.589	4.397	2.187	2.792
Sc_2AlC	3.274	14.590	4.456	2.252	3.072
Sc_2GaC	3.278	14.533	4.433	2.261	3.049
Sc_2InC	3.352	15.564	4.643	2.283	3.307
Sc_2TlC	3.328	15.096	4.536	2.275	3.197

Table S6. The lattice parameters of bulk M_3AC_2 and M_4AC_3 and bond lengths of M-C and M-A bonds (M= Ti, V, or Nb, A = Al, Si, Ga, Ge, or Sn).

M_3AC_2	a(Å)	c(Å)	c/a	$d_{M\text{-}C}$(Å)	$d_{M\text{-}A}$(Å)
Ti_3AlC_2	3.423	17.448	5.097	2.438,2.667	4.121
Ti_3SiC_2	3.051	17.487	5.731	2.173,2.084	2.065
Ti_3GeC_2	3.665	18.268	4.985	2.311,2.212	2.577
V_3AlC_2	3.073	18.556	6.038	2.046,2.113	2.941
Ti_4AlC_3	3.057	23.318	7.627	2.131,2.061,2.213	2.846
Ti_4GaC_3	3.064	22.997	7.505	2.136,2.216,2.062	2.790
Ti_4GeC_3	3.068	22.571	7.356	2.139,2.203,2.075	2.710
V_4AlC_3	2.894	22.569	7.798	2.077,2.031,1.982	2.712
Nb_4AlC_3	3.125	24.065	7.701	2.241,2.215,2.155	2.863

Table S7. Calculated exfoliation energy (in unit of eV/Å^2) of $M_{n+1}AC_n$ to $M_{n+1}C_n$ phases.

Systems	Al	Si	P	S	Ga	Ge	As	In	Sn	Tl	Pb
Cr_2AC	0.253	-	-	-	0.357	0.214	-	-	-	-	-
Hf_2AC	0.187	-	-	-	-	-	-	0.209	0.208	0.215	0.128
Mo_2AC	-	-	-	-	0.193	-	-	-	-	-	-
Nb_2AC	0.246	-	0.279	0.287	0.221	0.230	0.286	0.226	0.251	-	-
Sc_2AC	0.099	-	-	-	0.159	-	-	0.181	-	0.145	-
Ta_2AC	0.246	-	-	-	0.267	-	-	-	-	-	-
Ti_2AC	0.225	0.258	0.302	0.319	0.247	0.251	0.315	0.207	0.213	0.193	0.303
V_2AC	0.141	-	0.308		0.291	0.246	0.106	-	-	-	-
Zr_2AC	0.173	-	-	0.295	-	-	-	0.215	0.256	0.021	0.095
Ti_3AC_2	0.221	-	-	-	-	0.211	-	-	-	-	-
T_4AC_3	0.224	0.254	-	-	0.266	0.261	-	-	-	-	-
V_3AC_2	0.234	-	-	-	-	-	-	-	-	-	-
V_4AC_3	0.251	-	-	-	-	-	-	-	-	-	-
Nb_4AC_3	0.235	-	-	-	-	-	-	-	-	-	-

Table S8. Calculated binding energy of A in $M_{n+1}AC_n$ systems (eV).

Systems	Al	Si	P	S	Ga	Ge	As	In	Sn	Tl	Pb
Cr₂AC	-1.34	-	-	-	-2.93	-1.47	-	-	-	-	-
Hf₂AC	-1.43	-	-	-	-	-	-	-1.88	-1.93	-2.06	-1.28
Mo₂AC	-	-	-	-	-2.33	-	-	-	-	-	-
Nb₂AC	-1.99	-	-3.31	-2.94	-2.09	-1.71	-3.41	-2.01	-2.16	-	-
Sc₂AC	-0.34	-	-	-	-1.39	-	-	-1.55	-	-1.35	-
Ta₂AC	-2.08	-	-	-	-2.47	-	-	-	-	-	-
Ti₂AC	-1.48	-1.95	-3.05	-3.47	-2.04	-2.28	-3.38	-1.57	-1.74	-1.37	-2.67
V₂AC	-1.21	-	-2.96		-2.44	-2.06	-0.94	-	-	-	-
Zr₂AC	-1.24	-	-	-3.92	-	-	-	-1.33	-1.97	-1.62	-1.38
Ti₃AC₂	-1.47	-1.91	-	-	-	-3.38	-			-	-
T₄AC₃	-1.44	-	-	-	-2.14	-2.06	-	-	-	-	-
V₃AC₂	-1.94	-	-	-	-	-	-	-	-	-	-
V₄AC₃	-1.97	-	-	-	-	-	-	-	-	-	-
Nb₄AC₃	-1.99	-	-	-	-	-	-	-	-	-	-

Table S9. The calculated binding energy (E_b), formation energy of oxygen vacancy (E_f), and gained electrons (Ne) of surface O* of $M_3C_2O_2$, and adsorption free energy of atomic hydrogen (ΔG_{H*}) on the $M_3C_2O_2$ surface.

System	E_b (eV)	E_f (eV)	Ne (e)	ΔG_{H*} (eV)
Ti₃C₂O₂	-5.87	5.43	1.19	-0.33
V₃C₂O₂	-4.32	3.93	1.03	-0.47
Cr₃C₂O₂	-4.08	3.99	0.97	-0.55
Y₃C₂O₂	-4.31	3.42	1.26	-0.08
Zr₃C₂O₂	-5.61	5.55	1.29	0.16
Nb₃C₂O₂	-5.36	5.16	1.21	0.49
Mo₃C₂O₂	-3.98	2.71	1.05	-0.70
Hf₃C₂O₂	-5.34	4.91	1.31	0.55
Ta₃C₂O₂	-5.42	5.25	1.27	0.76
W₃C₂O₂	-3.39	2.39	1.14	-0.97

Table S10. The calculated binding energy (E_b), formation energy of oxygen vacancy (E_f), and gained electrons (Ne) of surface terminated O* of $M_4C_3O_2$, and adsorption free energy of atomic hydrogen (ΔG_{H*}) on the $M_4C_3O_2$ surface.

System	E_b (eV)	E_f (eV)	Ne (e)	ΔG_{H*} (eV)
$Ti_4C_3O_2$	-5.58	5.18	1.16	-0.30
$V_4C_3O_2$	-4.57	4.05	1.05	-0.44
$Cr_4C_3O_2$	-3.48	3.11	0.97	-0.87
$Y_4C_3O_2$	-4.91	3.45	1.28	-0.08
$Zr_4C_3O_2$	-6.24	5.84	1.30	0.27
$Nb_4C_3O_2$	-5.28	5.25	1.22	0.54
$Mo_4C_3O_2$	-3.89	3.21	1.05	-0.62
$Hf_4C_3O_2$	-5.47	4.63	1.31	0.48
$Ta_4C_3O_2$	-5.33	4.91	1.28	0.86
$W_4C_3O_2$	-3.12	2.11	1.14	-0.93

Table S11. Adsorption free energy of atomic hydrogen (ΔG_{H*}) (eV) on the M_2CO_2 surface at different hydrogen coverage.

System	ϑ=12.5%	ϑ=255	ϑ=37.5%	ϑ=50%
Ti_2CO_2	-0.24	0.09	0.68	0.96
V_2CO_2	-0.43	0.10	0.52	0.79
Cr_2CO_2	-0.47	-0.24	0.21	0.45
Y_2CO_2	0.07	0.13	0.22	0.55
Zr_2CO_2	0.18	0.98	1.21	1.33
Nb_2CO_2	0.41	0.76	0.97	1.19
Mo_2CO_2	-0.49	0.05	0.32	0.77
Hf_2CO_2	0.49	0.69	0.84	1.47
Ta_2CO_2	0.43	0.51	1.01	1.28
W_2CO_2	-0.11	0.59	0.96	1.14

Table S12. Adsorption energy (ΔE) on the M_2CO_2 surface for Heyrovsky and Tafel mechanisms.

System	Heyrovsky (eV)	Tafel (eV)
Ti_2CO_2	0.03	-0.58
V_2CO_2	-0.02	1.21
Cr_2CO_2	-0.03	-0.01
Y_2CO_2	-0.22	-1.92
Zr_2CO_2	0.01	-0.93
Nb_2CO_2	-0.01	-0.53
Mo_2CO_2	-0.09	-0.02
Hf_2CO_2	-0.05	-1.73
Ta_2CO_2	0.03	-1.26
W_2CO_2	0.01	-0.09

2. Supplementary analysis

2.1 DOS of 10 M_2CO_2 MXenes with considering the spin-polarized.

The total DOSs of 10 M_2CO_2 MXenes with considering the spin-polarization are calculated, results are presented in Figure S12. Like the results of Figure S12, there is a trend that for the same groups, the DOSs of spin-up and spin-down shift to lower energy with the groups increase from Ti to Cr, as illustration of the blue arrow in Figure S12. This trend is demonstrated by the results of p-DOS (Figure 5), for example, from Hf to W, the p-DOS shifts to lower energy.

2.2 The correlation between ΔG_{H*} and $\varepsilon_{p\text{-}\sigma}$

We have calculated fully filled bonding orbital (σ) center of surface O*, $\varepsilon_{p\text{-}\sigma}$ and correlation between adsorption free energy of atomic hydrogen (ΔG_{H*}) and $\varepsilon_{p\text{-}\sigma}$ is shown in Figure S13. It can be found that when the $\varepsilon_{p\text{-}\sigma}$ are in the range of -4.7~-3.9 eV, the absolute free Gibbs free energy$|\Delta G_{H*}|$is less than 0.3 eV (corresponding ε_p values are -4.1~-3.3 eV), which could deliver a better catalytic performances of MXenes for HER. The two descriptors are indicate that the Ti, V, Cr, Mo, and W based MXenes, which all lie in zone A in Figure 4 (in the revised manuscript) could possess superior HER catalytic performances (see in Figure R4) consistenting with the prediction based on Figure 4

2.3. Electronic structures of M_2CO_2 (lie in Zone B)

The electronic structures of V_2CO_2, Nb_2CO_2, Mo_2CO_2, W_2CO_2 (lie in Zone A) are further calculated and results are presented in Figure S14. It can be seen that four studied V_2CO_2, Nb_2CO_2, Mo_2CO_2, W_2CO_2 MXenes show metallic characteristics. Our previous work indicated that Cr_2CO_2 MXenes show metallic characteristics. Therefore, all of five studied M_2CO_2 MXenes lie in Zone and displayed metallic characteristics. The MXenes in Zone A with good electrical conductivity of favor it electron transfer during HER and therefore promote HER processes.